Applied Physics Letters ARTICLE pubs.aip.org/aip/apl

Plasma-induced optically active defects in hexagonal boron nitride

Cite as: Appl. Phys. Lett. **126**, 043103 (2025); doi: 10.1063/5.0253028
Submitted: 13 December 2024 · Accepted: 16 January 2025 ·
Published Online: 27 January 2025

F. Schaumburg,[a] D. Plitt, T. Wagner, N. Wöhrl, M. Geller, G. Prinz, and A. Lorke

AFFILIATIONS

Faculty of Physics and CENIDE, University of Duisburg-Essen, Lotharstr. 1, 47057 Duisburg, Germany

[a]Author to whom correspondence should be addressed: felix.schaumburg@uni-due.de

ABSTRACT

Hexagonal boron nitride (hBN) has been the subject of numerous research efforts in the last decade. Of particular interest is the creation of optically active defects in hBN because of their easy integration, e.g., in van der Waals heterostructures, and their room temperature photon emission. Many methods to create such defects in hBN are still under investigation. In this work, we present our approach to creating single defect emitters in hBN using remote plasma with different plasma species and report on the outcome statistically. We have used argon, nitrogen, and oxygen plasmas and report statistics on the emitters, produced by the different gas species and their optical properties. In particular, we examine the emission of the exfoliated flakes before and after the plasma processes without an annealing step to avoid creating emitters that are not caused by the plasma exposure. Our findings suggest that the purely physical argon plasma treatment is the most promising route for creating optically active defect emitters in hBN by plasma exposure.

The photonics of quantum emitters is an ongoing and important field of research. For example, single emitters are an essential part of quantum information technology, like quantum cryptography.[1–3] Another usage for single emitters is quantum sensing.[4–8] Several different materials have been suggested for such applications, such as diamond color centers[5,7,9,10] and self-assembled as well as colloidal quantum dots.[11–14] Recently, 2D-materials have also come into focus as possible hosts of single emitters,[15,16] where especially single-photon emitters are of interest for quantum communication.[17–20] One of them is hexagonal boron nitride (hBN). It can host defects that emit light even at room temperature similar to color centers in diamond[16–18,21–24] and has the advantage of easy integration into devices, because of its van der Waals structure that can be transferred and stacked into electro-optical active devices.[20,25–29] Research on how to spectrally and locally induce single defect emitters is still ongoing.[15,18,19,24,30,31] A promising method is plasma treatment of the hBN.[32–37] Here, we present a systematic study of how to produce defect emission in exfoliated hBN by the influence of plasma treatment using three specific species: argon, which will only interact physically with hBN; nitrogen as a constituent of boron nitride; and oxygen as a foreign and chemically reactive species. With our work, we want to make way to further understand the behavior of different plasmas not only statistically but also in direct comparison to each other.

The investigated samples were prepared as follows. Silicon wafer pieces ($5 \times 5\,\mathrm{mm}^2$) with a 100 nm thick SiO_2 layer were used as substrates. After cleaning with nitrogen gas, they were exposed to a strong oxygen plasma to remove any organic residues on the surface. Then hBN was exfoliated on the sample surface. This resulted in flakes with varying thicknesses, ranging from a few monolayers up to 200 nm. The thickness was roughly estimated from the color, observed in an optical microscope [see insets in Figs. 1(a), 1(d), and 1(g)]. Different thicknesses show different reflection and transmission due to thin-film interference.[38] Therefore, it can be estimated that the blue-greenish flake parts in the insets in Figs. 1(d) and 1(g) have a thickness of about 15 nm, and the flake in the inset in Fig. 1(a) has a thickness of around 110 nm.

The pristine flakes are optically characterized using spatially resolved scanning photoluminescence (PL) spectroscopy. The measurements were performed in a custom-built quasi-confocal[39] Raman/PL spectroscopy setup. We used a 50× objective (NA = 0.85), resulting in a spot size of around $1\,\mu\mathrm{m}^2$.[40] For the excitation, we used three different lasers: A 532 nm and a 405 nm semiconductor laser, as well as a 633 nm He–Ne laser. Most measurements were taken with the 532 nm laser. For the untreated flakes, typical maps of the brightness (averaged over 20 nm spectral width) are shown in Figs. 1(a), 1(d), and 1(g) for center wavelengths of 590 and two times 600 nm, respectively. The

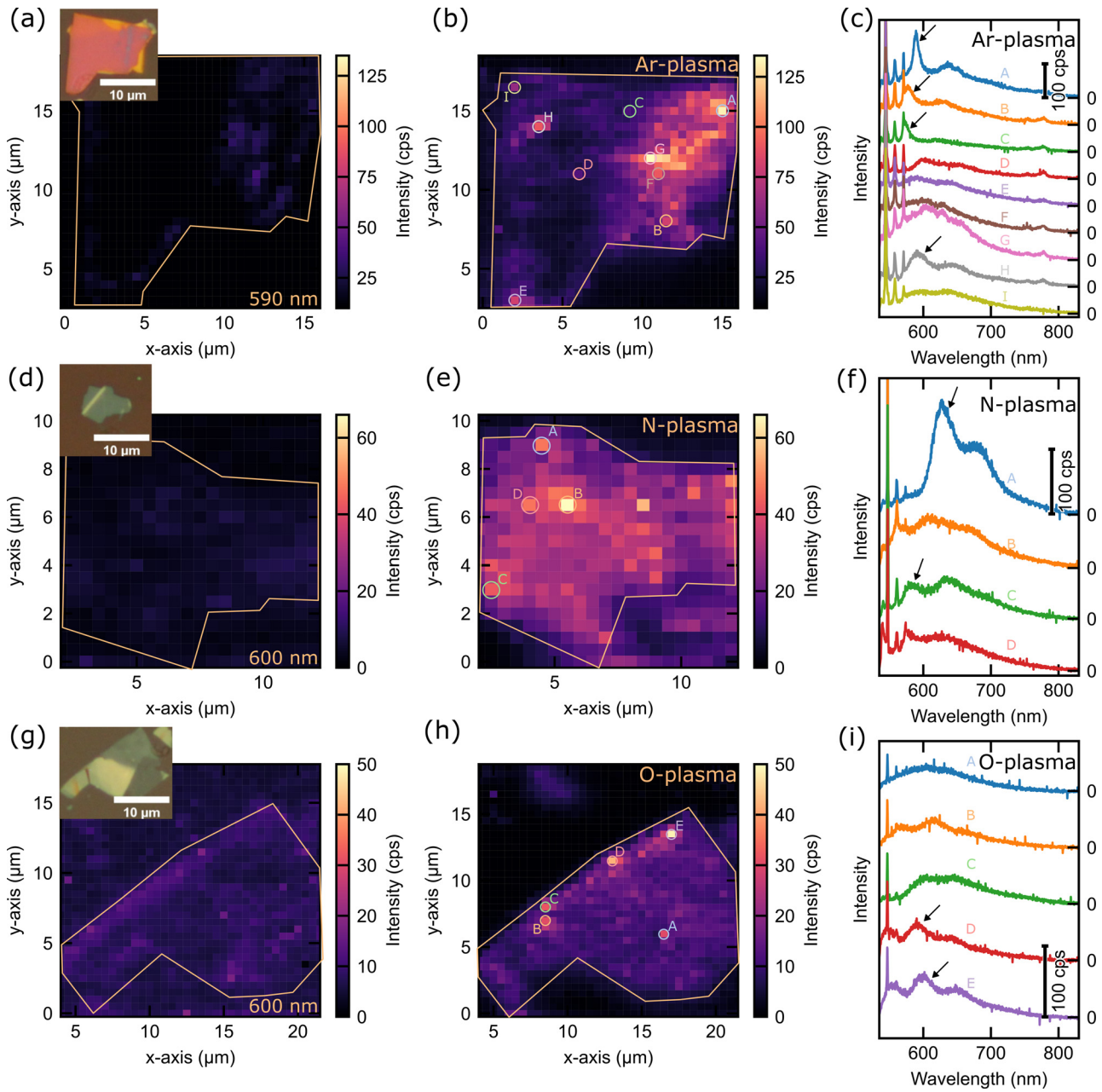

FIG. 1. Spatially resolved PL maps of hBN flakes before [(a), (d), and (g)] and after [(b), (e), and (h)] 90 s plasma treatment with PL spectra taken on chosen points from the maps (c), (f), and (i). The insets in (a), (d), and (g) show the flakes under an optical microscope. The text in the bottom right corner of (a), (d), and (g) shows the center wavelength chosen for every pair of PL maps [(a) and (b)], [(d) and (e)], and [(g) and (h)]. The flake shown in (a) and (b) was treated with an Ar plasma, the one in (d) and (e) with a N plasma, and the one in (g) and (h) with an O plasma. Every PL map pair has been plotted with the same intensity scale. The positions marked by circles and capital letters in the PL maps after the treatment (b), (e), and (h) correspond to the spectra shown in (c), (f), and (i), respectively. For clarity, the spectra in (c), (f), and (i) were shifted vertically in steps of 80 cps, and the peaks that we counted for the statistic are marked with black arrows. The optical transitions in the color centers are pumped with a 532 nm laser with an output power of 400 μW/μm^2. The CCD detector exposure time is set to 3 s.

false color brightness scales are chosen such that a direct comparison with the maps after the plasma treatment is possible. On these scales, all maps of the untreated samples appear mainly dark and show that there is only negligible defect emission from the pristine hBN flakes.

The characterized samples were then exposed to different gas species in a custom-built remote microwave plasma reactor. The remote nature of the system allows the treatment of surfaces at a distance from the excitation zone of the plasma. The distance is an important

additional parameter for controlling the plasma treatment because the chemical composition of the plasma changes with distance due to the different lifetimes of the excited species in the plasma. In addition, the parameter distance can also be used to control the intensity of the plasma treatment (and thus possibly the defect density generated).[41] The three gases used were argon (Ar), oxygen (O), and nitrogen (N). Argon is chemically inert and therefore only defects are introduced into the lattice by physical processes (collisions). It is also expected that this plasma treatment is the gentlest. Nitrogen and oxygen can both also lead to chemical processes and etching; however, while oxygen is a foreign species, nitrogen is already a component of the hBN material. Well-working parameters for the plasma exposure were a power of 600 W, a chamber pressure of 5 mbar, with a distance of 2 cm away from the resonator, and an exposure time of 90 s [Figs. 1(b), 1(e), and 1(h)].

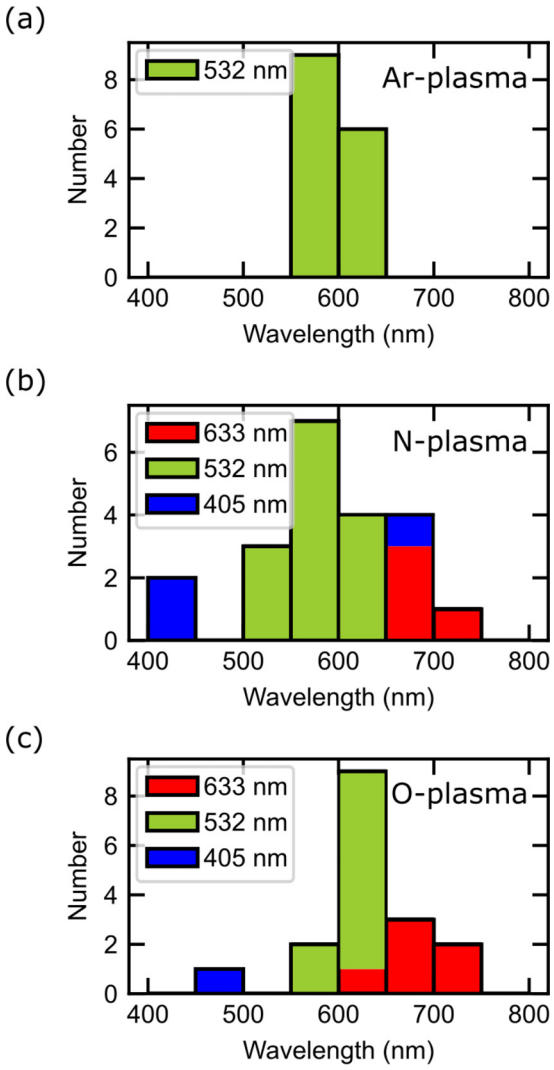

FIG. 2. Bar chart of the spectral distribution of the zero phonon line of emitters in hBN flakes after Ar (a), N (b), and O (c) plasma treatment. Bin size equals 50 nm.

Figures 1(b), 1(e), and 1(h) show the PL maps of the hBN flakes after exposure to argon, nitrogen, and oxygen, respectively. Note that identical flakes are shown in the parings (a → b), (d → e), and (g → h). This makes a direct comparison possible to identify the plasma-induced effects. For the same reason, we did not apply any annealing after the plasma treatment. Annealing has a stabilizing effect on the emitters;[37,42] however, it may also induce additional, non-plasma-related defects.[43–45]

We picked several particularly bright and spatially well-resolved spots on each plasma-exposed flake. Corresponding PL spectra of the positions marked in Figs. 1(b), 1(e), and 1(h) are shown in Figs. 1(c), 1(f), and 1(i). In total, about 100 flakes on 50 samples were characterized to get some statistics for the creation of defects. To identify individual emitters, we selected only spectra that had peaks with both high brightness ($\geq$ 25 cps) and narrow width (FWHM $<$ 30 nm). Typical examples marked with black arrows are seen in Fig. 1(c) (A, B, C, H), Fig. 1(f) (A, C), and Fig. 1(i) (D, E). Applying these criteria, a total of 50 separate defect emitters were identified.

Figures 2(a)–2(c) show the distribution of the emission wavelengths for argon, nitrogen, and oxygen, respectively. The colors correspond to the wavelength of the excitation laser: 405 nm (blue), 532 nm (green), and 633 nm (red). For argon exposure [Fig. 2(a)], emission is found only in a narrow region slightly below 600 nm and only from 532 nm excitation. The more chemically active species, nitrogen and oxygen, lead to a much broader range of emission energies [Figs. 2(b) and 2(c)]. This suggests that Ar exposure mainly induces a single kind of optically active defect, while N and O create a variety of color centers. In the high-bandgap material hBN, efficient defect excitation mainly occurs through phonon-assisted processes.[46] This explains why the luminescence around 580 nm is only observed under green laser illumination: the energy difference between excitation (2.33 eV) and emission (2.13 eV) corresponds well to the LO phonon energy in hBN (0.2 eV).[46,47] Luminescence at 580 nm is well-known in hBN.[48] Although its origin is still under debate,[49,50] it is often associated with the carbon complex defect $C_B N_B V_N$,[49–54] where, in combination with

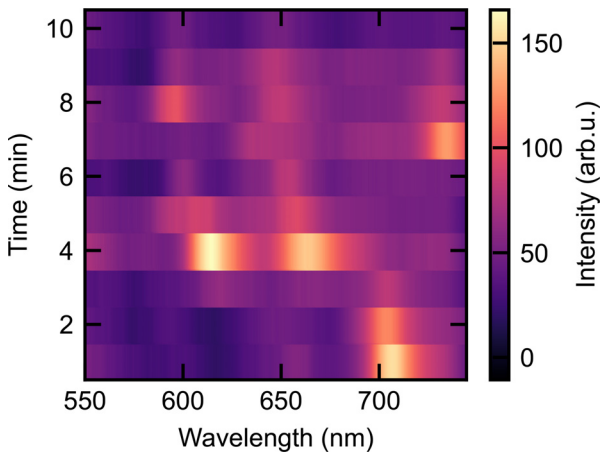

FIG. 3. Time-resolved PL emission series of a single defect on a nitrogen plasma-treated hBN flake. The x axis shows the spectral position, the y axis shows the time in 1 min steps, and the color indicates the intensity. The optical transitions in the color center are pumped with a 405 nm laser with an output power of 350 μW/μm^2. The CCD detector exposure time is set to 60 s.

a nitrogen vacancy, a carbon atom and a nitrogen atom each replace a boron atom. Even though we do not introduce any carbon in our plasma process, it cannot be ruled out that the hBN surface is contaminated with organic species as a source of carbon atoms, which are incorporated into the hBN through the Ar and N plasma exposure. The fact that emission around 580 nm is greatly reduced after oxygen exposure [Fig. 2(c)] supports this explanation, as oxygen plasma efficiently removes organic residue. Other possibilities for the 580 nm emission could be a nitrogen vacancy V_N, or a nitrogen vacancy in combination with an antisite defect $N_B V_N$.[49,50,53,54]

Quite a few defects with luminescence around or above 625 nm are also observed. These may originate from oxygen-based defects with

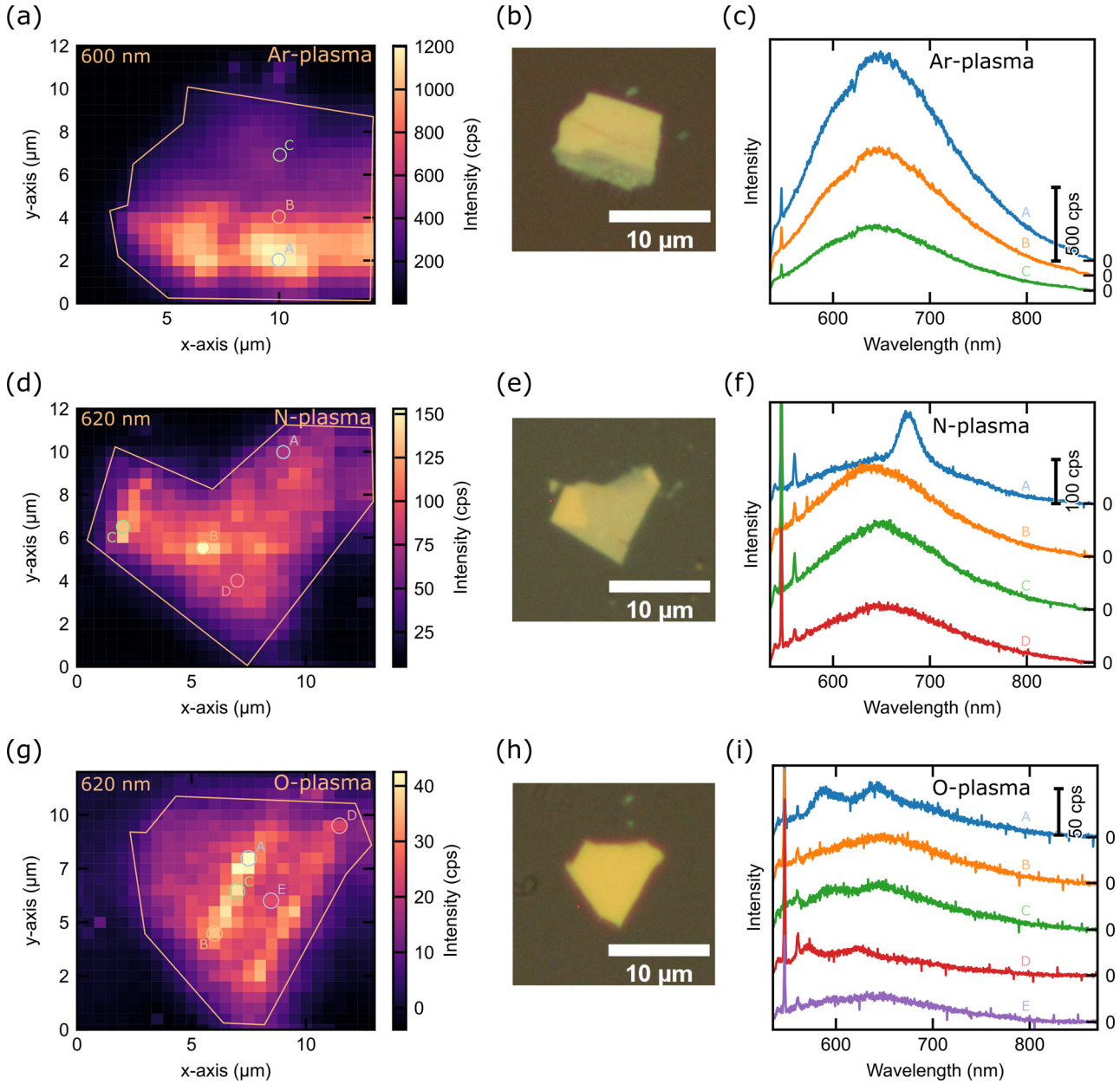

FIG. 4. PL maps (a), (d), and (g) of hBN flakes after treatment with plasma for 5 min, with the optical microscope images of the flakes (b), (e), and (h) and the spectra (c), (f), and (i) of the marked spots in the maps. The center wavelength of the PL maps (a), (d), and (g) are shown in their top left corner. The flake shown in (a)–(c) was treated with an Ar plasma, the one in (d)–(f) with a N plasma, and the one in (g)–(i) with an O plasma. For clarity, the spectra in (c), (f), and (i) were shifted vertically in steps of 100, 120, and 50 cps, respectively. The optical transitions in the color centers are pumped with a 532 nm laser with an output power of 400 $\mu W/\mu m^2$. The CCD detector exposure time is set to 3 s.

emission energies around or below 2 eV, such as an O_2 molecule in the vicinity of a boron vacancy O_2V_B or the oxygen complex $O_BO_BV_N$.[37,49,53,54] The fact that emission around 625 nm is particularly common for the oxygen-treated flakes, see Fig. 2(c), further supports this assignment.

The broader range of emission energies that are observed after N and O plasma treatment allows us to also observe defect emission under blue and red laser illumination, see color-coded bars in Figs. 2(b) and 2(c). For 633 nm excitation, the most likely emission wavelength is around 685 nm, a shift of 0.15 eV, somewhat less than the LO phonon energy that is observed for 532 nm excitation. For blue laser illumination, the statistics are insufficient to draw reliable conclusions. However, it is worth mentioning that in one incidence, the excitation and emission wavelengths (405 and 653 nm, respectively) correspond to an energy difference of as much as 1.16 eV.

This analysis shows that the purely physical interaction from the Ar plasma results in much better-defined optically active emitters, compared to N and O, which also interact chemically. Also, note that the maximum number for all three plasma species is around 600 nm, which indicates that these are optically emitting defects that can be induced independently of the plasma species.

Figure 3 shows the time-resolved PL measurement of a single defect that was found on a N plasma-treated sample. Clear intermittence of the peak intensity and position can be observed on the timescale of 1 min. Generally, such instability is an undesirable effect. On the one hand, the stability could be improved by annealing.[37,42] On the other hand, intermittent emission, or "blinking," as well as spectral hopping, is also a characteristic of single emitters.[12,55–58] Emitter agglomerates would not show such a distinct appearance and disappearance of the PL intensity unless it is assumed that they are electronically coupled or otherwise behave in a correlated fashion. It is important to acknowledge that, despite the blinking and spectral hopping being characteristics of single emitters, the single-photon characteristic of these emitters cannot be claimed in the absence of a $g^2(0)$ measurement. This is a subject for future studies. The characteristic double emission peaks, e.g., in minutes 4, 5, and 8, can be explained as the zero-phonon line and (separated by $\approx$160 meV) the phonon sideband.[47]

While singular light-emitting defects are of great interest for quantum information technologies, there is also application potential for homogeneous, bright, light-emitting materials. PL maps of strongly plasma-exposed flakes are shown in Figs. 4(a), 4(d), and 4(g). These flakes were exposed for 5 min and positioned closer to the plasma center (just inside the resonator), compared to the flakes in Fig. 1. These were positioned at the height of the resonator. Optical microscope images of these flakes are presented in Figs. 4(b), 4(e), and 4(h), respectively. In comparison with the maps in Fig. 1, somewhat smoother, large-scale intensity fluctuations are observed in Figs. 4(a), 4(d), and 4(g), as expected for the stronger plasma exposure. Comparing Figs. 4(i) and 1(i), no improvement of maximum count rates can be observed for extended O plasma treatment. This can be explained by an ablation effect[33,37,59,60] caused by the formation of volatile oxygen compounds on the surface.[60,61]

For strong N exposure, a roughly doubled light intensity is found [see Figs. 4(f) and 1(f)]. In the case of the strongly Ar plasma-treated flake [Fig. 4(c)], an up to 10 times higher signal compared to the weakly treated flakes [Fig. 1(c)] is observed. This again shows that Ar irradiation is superior to N or O plasma exposure for the generation of optically active defects. Note the strong difference in intensity between the lower and the upper part of the PL map in Fig. 4(a). Comparison with the optical image in Fig. 4(b) suggests that this is caused by the different thicknesses in these two areas. Following our previous work on optical properties of hBN flakes,[38] we attribute this intensity pattern to thin-film interference, which can increase or decrease light emission/extraction, depending on the ratio between flake thickness and wavelength.

In conclusion, we have studied the creation of optically active defects in hexagonal boron nitride by plasma exposure. Exfoliated hBN flakes on top of Si/SiO_2 substrates were introduced to a remote plasma. The gas species employed were argon, nitrogen, and oxygen. Single defects were created on samples irradiated for 90 s by a remote plasma. By precisely controlling the plasma treatment parameters, we were able to generate and optically characterize 50 individual emitters. The distribution of the emission wavelength of the different emitters was found to be narrower for exposure to Ar, compared to N or O. This shows that a purely physical plasma interaction results in better-defined color centers, giving the best control over the created defects. As an annealing step was intentionally omitted to avoid temperature-induced creation of defects, blinking effects and spectral hopping were observed. Samples that were irradiated for 5 min inside the plasma resonator exhibited broad and bright emission. Again, the best results, i.e., the brightest emission, were observed for the Ar process. The ablation effect of the oxygen plasma, as evidenced by previous studies,[33,37,59–61] led to a saturation of the emitter density. This suggests that the argon plasma process may be the most promising candidate for introducing defect emission, both in large ensemble structures and in singular defects. Future investigations may also explore the potential of a combined gas plasma process.

The funding by the Deutsche Forschungsgemeinschaft (DFG, German Research Foundation) within projects SFB 1242, ID No. 278162697, and IRTG 2803-461605777 is gratefully acknowledged.

AUTHOR DECLARATIONS

Conflict of Interest

The authors have no conflicts to disclose.

Author Contributions

F. Schaumburg: Conceptualization (lead); Data curation (equal); Formal analysis (equal); Investigation (equal); Methodology (equal); Project administration (equal); Software (equal); Supervision (equal); Validation (equal); Visualization (equal); Writing – original draft (equal); Writing – review & editing (equal). **D. Plitt:** Data curation (equal); Formal analysis (equal); Investigation (equal); Visualization (supporting); Writing – original draft (supporting); Writing – review & editing (supporting). **T. Wagner:** Conceptualization (equal); Investigation (equal); Methodology (equal); Supervision (equal); Validation (equal); Visualization (supporting); Writing – review & editing (supporting). **N. Wöhrl:** Conceptualization (equal); Funding acquisition (equal); Methodology (equal); Project administration (equal); Supervision (equal); Validation (equal); Writing – review & editing (supporting). **M. Geller:** Funding acquisition (equal); Methodology (equal); Project administration (equal); Supervision

(equal); Validation (equal); Writing – review & editing (equal). **G. Prinz:** Conceptualization (equal); Methodology (equal); Project administration (equal); Supervision (equal); Validation (equal); Visualization (equal); Writing – review & editing (equal). **A. Lorke:** Formal analysis (equal); Funding acquisition (equal); Methodology (equal); Project administration (lead); Resources (lead); Supervision (lead); Validation (equal); Visualization (equal); Writing – original draft (equal); Writing – review & editing (equal).

DATA AVAILABILITY

The data that support the findings of this study are available from the corresponding author upon reasonable request.

REFERENCES

[1]M. Bozzio, M. Vyvlecka, M. Cosacchi, C. Nawrath, T. Seidelmann, J. C. Loredo, S. L. Portalupi, V. M. Axt, P. Michler, and P. Walther, npj Quantum Inf. **8**, 104 (2022).
[2]M. Zahidy, M. T. Mikkelsen, R. Müller, B. Da Lio, M. Krehbiel, Y. Wang, N. Bart, A. D. Wieck, A. Ludwig, M. Galili, S. Forchhammer, P. Lodahl, L. K. Oxenløwe, D. Bacco, and L. Midolo, npj Quantum Inf. **10**, 6 (2024).
[3]M. W. Doherty, C. R. Du, and G. D. Fuchs, J. Appl. Phys. **131**, 010401 (2022).
[4]C. L. Degen, F. Reinhard, and P. Cappellaro, Rev. Mod. Phys. **89**, 035002 (2017).
[5]D. Kim, M. I. Ibrahim, C. Foy, M. E. Trusheim, R. Han, and D. R. Englund, Nat. Electron. **2**, 284 (2019).
[6]M. Kutas, B. Haase, P. Bickert, F. Riexinger, D. Molter, and G. Von Freymann, Sci. Adv. **6**, 8065 (2020).
[7]P. Rembold, N. Oshnik, M. M. Müller, S. Montangero, T. Calarco, and E. Neu, AVS Quantum Sci. **2**, 024701 (2020).
[8]Z. Zhang and Q. Zhuang, Quantum Sci. Technol. **6**, 043001 (2021).
[9]Z. Ju, J. Lin, S. Shen, B. Wu, and E. Wu, Adv. Phys.: X **6**, 1858721 (2021).
[10]F. Jelezko and J. Wrachtrup, Phys. Status Solidi A **203**, 3207 (2006).
[11]J. M. Moison, F. Houzay, F. Barthe, L. Leprince, E. André, and O. Vatel, Appl. Phys. Lett. **64**, 196 (1994).
[12]M. H. Stopel, J. C. Prangsma, C. Blum, and V. Subramaniam, RSC Adv. **3**, 17440 (2013).
[13]Y. S. Park, S. Guo, N. S. Makarov, and V. I. Klimov, ACS Nano **9**, 10386 (2015).
[14]E. Kleinherbers, H. Mannel, J. Kerski, M. Geller, A. Lorke, and J. König, Phys. Rev. Res. **5**, 043103 (2023).
[15]A. Micevic, N. Pettinger, A. Hötger, L. Sigl, M. Florian, T. Taniguchi, K. Watanabe, K. Müller, J. J. Finley, C. Kastl, and A. W. Holleitner, Appl. Phys. Lett. **121**, 183101 (2022).
[16]N. J. Guo, W. Liu, Z. P. Li, Y. Z. Yang, S. Yu, Y. Meng, Z. A. Wang, X. D. Zeng, F. F. Yan, Q. Li, J. F. Wang, J. S. Xu, Y. T. Wang, J. S. Tang, C. F. Li, and G. C. Guo, ACS Omega **7**, 1733 (2022).
[17]T. T. Tran, K. Bray, M. J. Ford, M. Toth, and I. Aharonovich, Nat. Nanotechnol. **11**, 37 (2016).
[18]F. Hayee, L. Yu, J. L. Zhang, C. J. Ciccarino, M. Nguyen, A. F. Marshall, I. Aharonovich, J. Vučković, P. Narang, T. F. Heinz, and J. A. Dionne, Nat. Mater. **19**, 534 (2020).
[19]K. Parto, S. I. Azzam, K. Banerjee, and G. Moody, Nat. Commun. **12**, 3585 (2021).
[20]S. I. Azzam, K. Parto, and G. Moody, Appl. Phys. Lett. **118**, 240502 (2021).
[21]C. Cholsuk, A. Zand, A. Çakan, and T. Vogl, J. Phys. Chem. C **128**, 12716 (2024).
[22]A. Kumar, C. Cholsuk, A. Zand, M. N. Mishuk, T. Matthes, F. Eilenberger, S. Suwanna, and T. Vogl, APL Mater. **11**, 071108 (2023).
[23]A. Kumar, Samaner, C. Cholsuk, T. Matthes, S. Paçal, Y. Oyun, A. Zand, R. J. Chapman, G. Saerens, R. Grange, S. Suwanna, S. Ateş, and T. Vogl, ACS Nano **18**(7), 5270–5281 (2023).
[24]A. Kumar, C. Cholsuk, M. N. Mishuk, M. Hazra, C. Pillot, T. Matthes, T. A. Shaik, A. Çakan, V. Deckert, S. Suwanna, and T. Vogl, ACS Appl. Opt. Mater. **2**, 323 (2024).
[25]J. Yu, X. Kuang, J. Zhong, L. Cao, C. Zeng, J. Ding, C. Cong, S. Wang, P. Dai, X. Yue, Z. Liu, and Y. Liu, Opt. Express **28**, 13260 (2020).
[26]A. K. Geim and I. V. Grigorieva, Nature **499**, 419 (2013).
[27]A. Castellanos-Gomez, X. Duan, Z. Fei, H. R. Gutierrez, Y. Huang, X. Huang, J. Quereda, Q. Qian, E. Sutter, and P. Sutter, Nat. Rev. Methods Primers **2**, 58 (2022).
[28]S. J. White, T. Yang, N. Dontschuk, C. Li, Z. Q. Xu, M. Kianinia, A. Stacey, M. Toth, and I. Aharonovich, Light **11**, 1–9 (2022).
[29]O. Karni, E. Barré, S. C. Lau, R. Gillen, E. Y. Ma, B. Kim, K. Watanabe, T. Taniguchi, J. Maultzsch, K. Barmak, R. H. Page, and T. F. Heinz, Phys. Rev. Lett. **123**, 247402 (2019).
[30]Y. Xia, Q. Li, J. Kim, W. Bao, C. Gong, S. Yang, Y. Wang, and X. Zhang, Nano Lett. **19**, 7100 (2019).
[31]A. R.-P. Montblanch, M. Barbone, I. Aharonovich, M. Atatüre, and A. C. Ferrari, Nat. Nanotechnol. **18**, 555 (2023).
[32]M. S. Kim, G. Nam, S. Park, H. Kim, G. H. Han, J. Lee, K. P. Dhakal, J. Y. Leem, Y. H. Lee, and J. Kim, Thin Solid Films **590**, 318–323 (2015).
[33]Y. S. Na, J. H. Kim, S. Kang, J. H. Jeong, S. Park, D. H. Kim, K. Ihm, K. Watanabe, T. Taniguchi, Y. K. Kwon, Y. D. Kim, and G. H. Lee, 2D Mater. **8**, 045041 (2021).
[34]Z. Wu and Z. Ni, Nanophotonics **6**, 1219 (2017).
[35]L. Zeng, S. Zhang, J. Meng, J. Chen, J. Jiang, Y. Shi, J. Huang, Z. Yin, J. Wu, and X. Zhang, ACS Appl. Mater. Interfaces **16**, 24899 (2024).
[36]J. Jiang, T. Xu, J. Lu, L. Sun, and Z. Ni, Research **2019**, 10.
[37]Z. Q. Xu, C. Elbadawi, T. T. Tran, M. Kianinia, X. Li, D. Liu, T. B. Hoffman, M. Nguyen, S. Kim, J. H. Edgar, X. Wu, L. Song, S. Ali, M. Ford, M. Toth, and I. Aharonovich, Nanoscale **10**, 7957 (2018).
[38]F. Schaumburg, S. Sleziona, M. Zöllner, V. Dergianlis, M. Schleberger, M. Geller, A. Lorke, and G. Prinz, Appl. Phys. Lett. **123**, 073101 (2023).
[39]Note: For a confocal geometry, in the strict sense, an aperture (or equivalently an optical fiber) is necessary in the detection path. This ensures that the excitation and detection are identical not only laterally (x-y direction) but also along the z axis. For free-beam optics, it is not uncommon that the input slit of the spectrometer serves as an aperture, however, only in one dimension. We therefore used the term "quasi-confocal."
[40]A. Asaithambi, R. Kozubek, G. M. Prinz, F. Reale, E. Pollmann, M. Ney, C. Mattevi, M. Schleberger, and A. Lorke, Phys. Status Solidi - RRL **15**, 2000466 (2021).
[41]T. Wagner, F. Schaumburg, F. Kensy, A. Lorke, and N. Wöhrl, "Changes: Optimizing morphology and chemistry of Nickel surfaces by a scalable plasma process for hydrogen electrolyzers," Surface Coatings Technol. (submitted).
[42]J. C. Stewart, Y. Fan, J. S. Danial, A. Goetz, A. S. Prasad, O. J. Burton, J. A. Alexander-Webber, S. F. Lee, S. M. Skoff, V. Babenko, and S. Hofmann, ACS Nano **15**, 13591 (2021).
[43]T. T. Tran, C. Elbadawi, D. Totonjian, C. J. Lobo, G. Grosso, H. Moon, D. R. Englund, M. J. Ford, I. Aharonovich, and M. Toth, in *Conference on Lasers and Electro-Optics (CLEO 2017)* (Institute of Electrical and Electronics Engineers Inc., 2017), pp. 1–2.
[44]C. Lyu, Y. Zhu, P. Gu, J. Qiao, K. Watanabe, T. Taniguchi, and Y. Ye, Appl. Phys. Lett. **117**, 244002 (2020).
[45]Y. Chen, A. Gale, K. Yamamura, J. Horder, A. Condos, K. Watanabe, T. Taniguchi, M. Toth, and I. Aharonovich, Appl. Phys. Lett. **123**, 041902 (2023).
[46]J. A. Preuss, D. Groll, R. Schmidt, T. Hahn, P. Machnikowski, R. Bratschitsch, T. Kuhn, S. Michaelis De Vasconcellos, and D. Wigger, Optica **9**, 522 (2022).
[47]S. Reich, A. C. Ferrari, R. Arenal, A. Loiseau, I. Bello, and J. Robertson, Phys. Rev. B **71**, 205201 (2005).
[48]N. Mendelson, Z.-Q. Xu, T. T. Tran, M. Kianinia, J. Scott, C. Bradac, I. Aharonovich, and M. Toth, ACS Nano **13**, 3132 (2019).
[49]S. A. Tawfik, S. Ali, M. Fronzi, M. Kianinia, T. T. Tran, C. Stampfl, I. Aharonovich, M. Toth, and M. J. Ford, Nanoscale **9**, 13575 (2017).
[50]M. Abdi, J.-P. Chou, A. Gali, and M. B. Plenio, ACS Photonics **5**, 1967 (2018).
[51]S. H. Kim, K. H. Park, Y. G. Lee, S. J. Kang, Y. Park, and Y. D. Kim, Nanomaterials **13**, 2344 (2023).
[52]A. Sajid and K. S. Thygesen, 2D Mater. **7**, 031007 (2020).
[53]M. Krečmarová, R. Canet-Albiach, H. Pashaei-Adl, S. Gorji, G. Muñoz-Matutano, M. Nesládek, J. P. Martínez-Pastor, and J. F. Sánchez-Royo, ACS Appl. Mater. Interfaces **13**, 46105 (2021).
[54]A. Sajid, J. R. Reimers, and M. J. Ford, Phys. Rev. B **97**, 064101 (2018).

[55]P. Tonndorf, R. Schmidt, R. Schneider, J. Kern, M. Buscema, G. A. Steele, A. Castellanos-Gomez, H. S. J. van der Zant, S. Michaelis de Vasconcellos, and R. Bratschitsch, Optica **2**, 347 (2015).
[56]C. Galland, Y. Ghosh, A. Steinbrück, M. Sykora, J. A. Hollingsworth, V. I. Klimov, and H. Htoon, Nature **479**, 203 (2011).
[57]F. D. Stefani, J. P. Hoogenboom, and E. Barkai, Phys. Today **62**(2), 34 (2009).
[58]K. L. Wustholz, E. D. Bott, B. Kahr, and P. J. Reid, J. Phys. Chem. C **112**, 7877 (2008).
[59]Y. Chen, C. Li, S. White, M. Nonahal, Z. Q. Xu, K. Watanabe, T. Taniguchi, M. Toth, T. T. Tran, and I. Aharonovich, ACS Appl. Mater. Interfaces **13**, 47283 (2021).
[60]S. Grenadier, J. Li, J. Lin, and H. Jiang, J. Vac. Sci. Technol. A **31**, 061517 (2013).
[61]L. F. Voss, C. E. Reinhardt, R. T. Graff, A. M. Conway, R. J. Nikolić, N. Deo, and C. L. Cheung, Nucl. Instrum. Methods Phys. Res, Sect. A **606**, 821 (2009).